





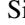






Hubble Space Telescope Reveals Spectacular Light Echoes Associated with the Stripped-envelope Supernova 2016adj in the Iconic Dust Lane of Centaurus A

Maximilian D. Stritzinger¹ , Francesco Taddia¹ , Stephen S. Lawrence² , F. Patat³ , Morgan Fraser⁴ , Lluís Galbany^{5,6} , Simon Holmbo¹ , Ali Hyder^{2,7} , and Emir Karamahmetoglu¹ 

¹ Department of Physics and Astronomy, Aarhus University, Ny Munkegade 120, DK-8000 Aarhus C, Denmark; max@phys.au.dk

² Dept. of Physics & Astronomy, 151 Hofstra University, Hempstead, NY 11549, USA

³ European Organization for Astronomical Research in the Southern Hemisphere (ESO), Karl-Schwarzschild-Str. 2, D-85748, Garching b. München, Germany

⁴ School of Physics, O'Brien Centre for Science North, University College Dublin, Belfield, Dublin 4, Ireland

⁵ Institute of Space Sciences (ICE, CSIC), Campus UAB, Carrer de Can Magrans, s/n, E-08193 Barcelona, Spain

⁶ Institut d'Estudis Espacials de Catalunya (IEEC), E-08034 Barcelona, Spain

⁷ Department of Astronomy, New Mexico State University, PO BOX 30001, MSC 4500, Las Cruces, NM 88003-8001 USA

Received 2022 July 10; revised 2022 September 19; accepted 2022 September 20; published 2022 October 27

Abstract

We present a multiband sequence of Hubble Space Telescope images documenting the emergence and evolution of multiple light echoes (LEs) linked to the stripped-envelope supernova (SN) 2016adj located in the central dust lane of Centaurus A. Following point-spread function subtraction, we identify the earliest LE emission associated with an SN at only +34 days past the epoch of the *B*-band maximum. Additional HST images taken on +1991 days reveal not only LE1 but also segments of a new inner LE ring (LE2) as well as two additional outer LE rings (LE3 and LE4). Adopting the single-scattering formalism, the angular radii of the LEs suggest they originate from discrete dust sheets in the foreground of the SN. This information, combined with measurements of color and optical depth of the scattering surfaces, informs a scenario with multiple sheets of clumpy dust characterized by a varying degree of holes. In this case, the larger the LE's angular radii, the farther in the foreground of the SN its dust sheet is located. However, an exception to this is LE2, which is formed by a dust sheet located in closer proximity to the SN than the dust sheets producing LE1, LE3, and LE4. The delayed appearance of LE2 can be attributed to its dust sheet having a significant hole along the line of sight between the SN and Earth.

Unified Astronomy Thesaurus concepts: [Type Ic supernovae \(1730\)](#); [Core-collapse supernovae \(304\)](#)

Supporting material: animation

1. Introduction

Light echoes (LEs) are produced when photons emitted by a transient source scatter off interstellar dust clouds (see Sugerman 2003, and references therein). Often appearing as arcs or wisps of light, LEs were first detected in Galactic and extragalactic novae over a hundred years ago (Kapteyn 1901; Ritchey 1901; Swope 1940) and successfully explained as scattering phenomena by Couderc (1939). Later, LEs were found around variable stars (Havlen 1972; Bond et al. 2003; Rest et al. 2012), while more recently, LEs associated with historical supernovae (SNe) have been documented (Rest et al. 2008, 2011; Vogt et al. 2012). Beginning with SN 1987A (Crotts 1988; Suntzeff et al. 1988), LE emission has been documented in a dozen nearby SNe (see Yang et al. 2017, and references therein).

In principle, measurements of the angular radius (α) of a LE as projected on the sky, along with the surface brightness, color evolution, and polarization signatures, provide a means to infer the structure, geometry, and extinction properties of the underlying dust including grain size and composition (Couderc 1939; Chevalier 1986; Patat 2005). Studies of SN 1987A (Xu et al. 1995) and SN 2014J (Yang et al. 2017) reveal multi-component LEs consisting of bright arcs with knot-like

structures superposed on more diffuse, full-ring emission. Reconstructed 3D dust mappings of both objects suggest the arcs and rings are produced by discrete slabs of interstellar dust, characterized by different thicknesses, column densities, and extinction properties (Xu et al. 1995; Yang et al. 2017).

We present a time series of multiband images taken with the Hubble Space Telescope (HST) of SN 2016adj nestled in the iconic dust lane of NGC 5128, hereafter Cen A (Hyder et al. 2018). The data document four distinct LE components that emerge at different times and which are associated with distinct sheets of dust. Our analysis of the LEs characterizes the locations and properties of the various sheets of dust producing the echoes.

BOSS (Backyard Observatory Supernova Search) discovered SN 2016adj on 2016 February 08.56 UT (i.e., JD–2,457,427.06) with $m_V = 14$ mag (Kiyota et al. 2016; Marples et al. 2016). Spectra obtained soon after discovery indicated it was a core-collapse SN, with reports differing in the subtype, i.e., SN II (Yi et al. 2016), SN Ib (Stritzinger et al. 2016), or SN IIb (Hounsell et al. 2016; Thomas et al. 2016). Banerjee et al. (2018) presented a near-infrared (NIR) spectral sequence of SN 2016adj and focused on modeling early carbon monoxide emission. Although Banerjee et al. adopted an SN IIb classification, they did note a lack of hydrogen and helium lines in their spectra. In a forthcoming paper (M. D. Stritzinger et al. 2023, in preparation), we establish the optical/NIR spectra of SN 2016adj are fully consistent with those of carbon-rich SNe Ic (Valenti et al. 2008; Shahbandeh et al. 2022).



Original content from this work may be used under the terms of the [Creative Commons Attribution 4.0 licence](#). Any further distribution of this work must maintain attribution to the author(s) and the title of the work, journal citation and DOI.

Table 1
Log of the HST+WFC3 Observations of SN 2016adj

Epoch	Image ID	Proposal No.	UT date	Phase ^a (d)	Total Integration (s)	Filter
0 ^b	ib6wrap1q	11360	2010-07-17 11:33:33	−2039	1605	F438W
	ib6wrciyq	11360	2010-07-06 13:40:17	−2049	1250	F547M
	ib6wrcjyq	11360	2010-07-06 18:15:43	−2049	1240	F814W
1	icvy01010	14115	2016-02-22 01:26:29	7	120	F438W
	icvy01020	14115	2016-02-22 01:47:16	7	120	F438W
	icvy01030	14115	2016-02-22 01:49:43	7	40	F814W
	icvy01040	14115	2016-02-22 01:51:30	7	40	F814W
	icvy01050	14115	2016-02-22 01:53:17	7	40	F814W
	icvy01060	14115	2016-02-22 01:55:04	7	40	F814W
2	id3q01010	14487	2016-03-19 23:15:45	34	1400	F438W
	id3q01020	14487	2016-03-19 23:42:47	34	100	F547M
	id3q01030	14487	2016-03-20 00:38:10	34	1200	F547M
	id3q01040	14487	2016-03-20 01:01:53	34	1200	F814W
	id3q01050	14487	2016-03-20 02:08:28	34	120	F814W
	id3q01060	14487	2016-03-20 02:22:51	34	300	F547M
3	id3q02010	14487	2016-04-29 15:11:42	75	1200	F547M
	id3q02020	14487	2016-04-29 15:35:28	75	1388	F438W
4	id3q03010	14487	2016-06-25 23:11:58	132	1200	F547M
	id3q03020	14487	2016-06-26 00:17:43	132	1388	F438W
5	id6h04010	14700	2016-12-12 18:30:25	302	1600	F547M
	id6h04020	14700	2016-12-12 19:00:48	302	1388	F814W
	id6h04030	14700	2016-12-12 20:09:57	302	2500	F438W
6	id6h05010	14700	2017-04-01 09:38:47	412	1600	F547M
	id6h05020	14700	2017-04-01 10:52:12	412	1388	F814W
	id6h05030	14700	2017-04-01 11:19:06	412	2500	F438W
7	id6h06010	14700	2017-09-15 02:01:24	578	1600	F547M
	id6h06020	14700	2017-09-15 02:31:47	578	1388	F814W
	id6h06030	14700	2017-09-15 03:42:13	578	2500	F438W
8	ieb310010	16179	2021-07-28 13:14:53	1991	780	F438W
	ieb310020	16179	2021-07-28 13:24:06	1991	720	F555W

Notes.

^a Days relative to the epoch of the *B*-band maximum estimated to have occurred on $\text{JD} - 2,457,433.47 \pm 2.0$. (see M. D. Stritzinger et al. 2023, in preparation).

^b Epoch 0 corresponds to pre-SN imaging used as host-galaxy templates to subtract host contamination from each science image.

2. HST Observations of SN 2016adj

HST observed SN 2016adj over eight epochs extending from 2016 February 22 to 2021 July 28 with the Wide Field Camera 3 (+WFC3). Drizzled HST frames were retrieved from the Mikulski Archive for Space Telescopes, consisting of eight, six, and five epochs taken with the F438W, F547M, and F814W filters, respectively, and a single epoch with the F555W filter. A summary of the HST images used in this study is provided in Table 1. This includes image IDs, program identification numbers, date of observations, phase relative to the epoch of the *B*-band maximum, exposure times, and filter identifications. The dates of observations correspond to +7 days and +1991 days past the epoch of the *B*-band maximum.⁸ In addition to the HST science

images, multiband HST images of the host taken during 2010 were used to perform galaxy-template subtraction on each of the post-SN images.

3. Results

3.1. The Light Echoes of SN 2016adj

A montage of template-subtracted HST images of SN 2016adj shown in Figure 1 reveals four distinct LE components present at various epochs.⁹ LE1 is first visually apparent as a half-ring on +75 days with a projected angular radius on the sky of $\alpha = 0''.27 \pm 0''.01$. The intensity of the half-ring LE is maximum at a position angle (PA) corresponding to the north and decreases until almost disappearing toward the west and east directions. Following Sugerma & Lawrence (2016), LE1

⁸ The epoch of the *B*-band maximum is estimated from a *B*-band light curve of SN 2016adj obtained by the Carnegie Supernova Project to have occurred on 2016 February 15 (i.e., $\text{JD} - 2,457,433.5 \pm 2$; M. D. Stritzinger et al. 2023, in preparation).

⁹ An animation of LE1 of SN 2016adj can viewed here: www.dropbox.com/s/1cp5uehx6d0qas7/SN_light_echo_evolution.gif?dl=0.

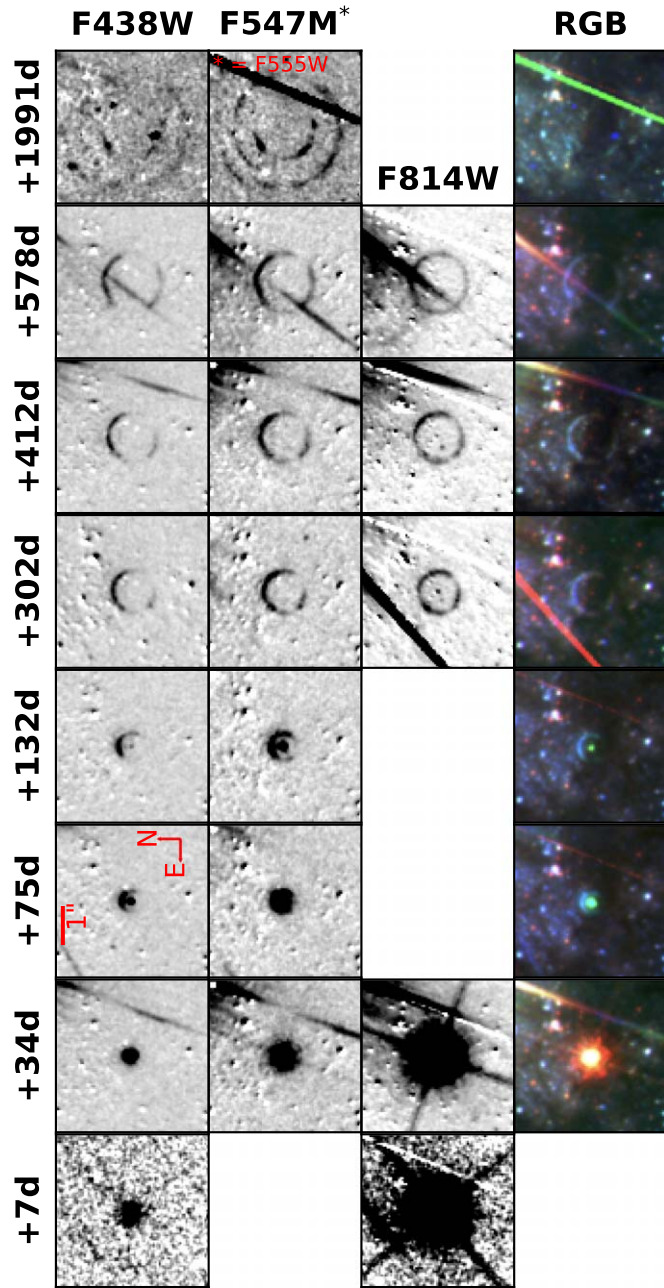


Figure 1. A montage of galaxy-subtracted HST images of SN 2016adj extending +7 days to +1991 days after the epoch of the B -band maximum. The F438W- (first row), F547M- (second row), and F814W-band (third row) images reveal the emergence and evolution of multiple LEs. Corresponding RGB composite images are presented in the bottom row. The LE (hereafter LE1) first appearing as a half-ring in the +34 day data (see Appendix) becomes visually apparent on +75 days and continues to radially expand through +1991 days. The most recent HST images also reveal a new partial inner LE ring (hereafter LE2), as well as LE segments of two additional outer rings located beyond LE1 and designated LE3 and LE4 (see also Figure 2). The SN position is centered in each of the $(4''/36 \times 4''/36)$ panels and is no longer visually apparent by +302 days. Many of the images are contaminated with a conspicuous saturation spike associated with a foreground star. Finally, the RGB composite images were used to construct an animation highlighting the time evolution of LE1. (An animation of this figure is available.)

is recovered in the +34 day F438W-band image as described in Appendix A.1 and shown in Figure A1. To our knowledge, this is the earliest detection of an LE surrounding an SN. Turning to epochs of +132 days and later, while the SN has faded, LE1

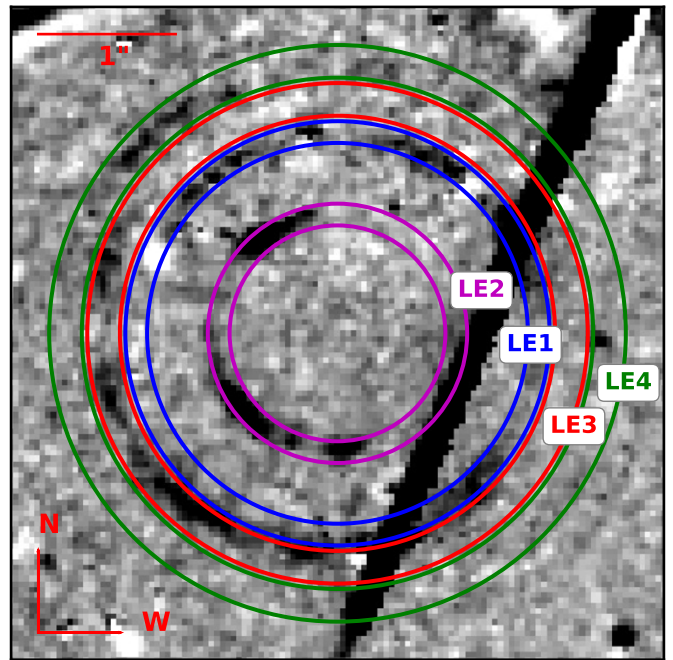


Figure 2. Host-subtracted F555W-band HST image of SN 2016adj on +1991 days, with the positions of LE1, LE2, LE3, and LE4 highlighted by colored rings and labeled.

continues to appear as a radially expanding ring with a nonuniform surface brightness out to +1991 days. As highlighted in Figure 2, the final epoch reveals additional LE components including an “inner” LE ring labeled LE2, which lies inside LE1, and segments of two “outer” rings designated LE3 and LE4.

Values of α for each LE component were measured following the procedure described in Appendix A.2, and the results are listed in Table A1. A linear fit to α as measured for LE1 over seven epochs reveals an expansion velocity of $0''.018$ per month. This translates to the superluminal value of $\sim 12c$, which is 0.75 times the value inferred for SN 1987A (Suntzeff et al. 1988). Furthermore, by fitting α between the first three epochs, we obtain an impressive superluminal value of $\sim 37c$.

3.2. Integrated Brightness and Color Evolution

To measure the LE brightness from the montage of data, the point-spread function (PSF) of the SN was first removed from the F438W and F547M images taken on +34 days and +75 days. PSF subtraction was performed by making use of tools within the *Astropy* *photutils* library (Bradley et al. 2020). To do so, a model PSF was constructed based on the PSFs of two dozen isolated field stars. The model PSF was scaled to the peak SN and LE signal and then subtracted, revealing the LE signal. Next, template images from 2010 were subtracted from all science images, and then photometry was computed for each LE component using two apertures centered on the SN position with radii respectively larger and smaller than the LE radius (e.g., Figure A1). The flux level of the innermost aperture was subtracted from that of the outermost aperture, yielding the LE flux. Integrated LE flux measurements (and magnitudes) of LE1–LE4 determined from the entire sequence of images are listed in Table A1, with uncertainties derived from the standard deviation of the background next to the ring. Flux values and the apparent

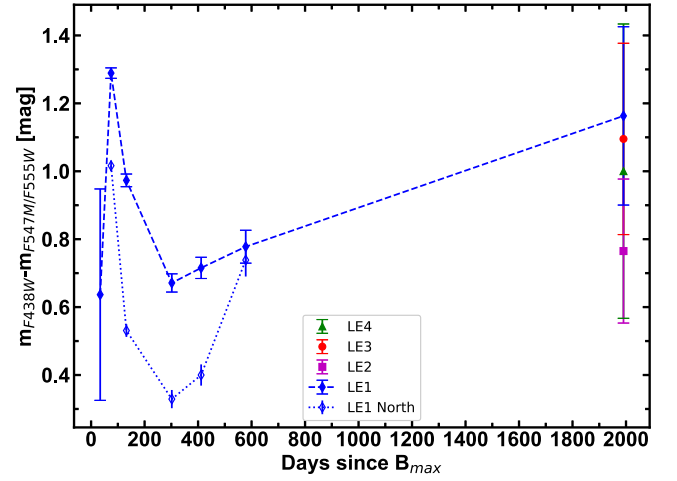
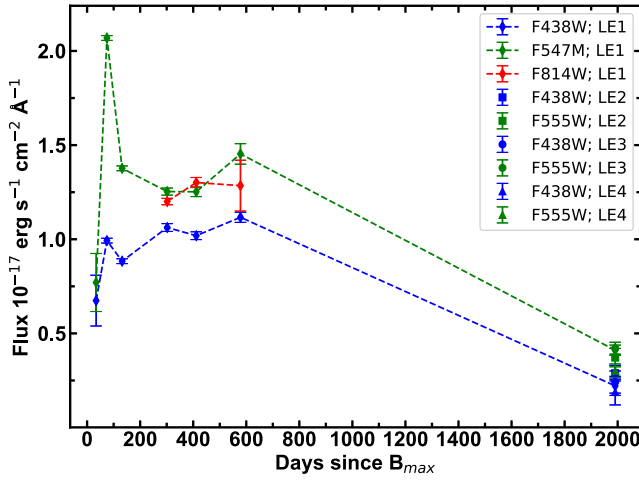


Figure 3. Left: multiband integrated flux evolution of LE1, as well as flux measurements of LE2–LE4 on +1991 days. Right: apparent ($m_{F438W} - m_{F547M}$) color evolution of LE1, and colors of LE2–LE4 (last epoch corresponds to $m_{F438W} - m_{F555W}$). Also plotted is the color of LE1 estimated from the segment of its ring extending over the north direction and which is clearly bluer (see Figure A3) than the color inferred from the total integrated flux.

colors for each LE component are plotted in Figure 3. In Figure A2 the flux of LE1 as measured from +75 days to +1991 days is plotted vs. PA in the top row, while the bottom row displays the F438W and F546M flux ratios.

Inspection of the left panel of Figure 3 reveals that on +34 days, LE1 exhibits similar flux values in both bands. Interestingly, while by +75 days the flux in the F438W band only slightly increases, in the F547M band its brightness increases by 1.3 ± 0.2 mag. This results in the color evolving to red over the same time period reaching a value of 1.3 mag on +75 days. Beyond +75 days and +302 days, as the flux in the F547M decreases and that of the F438W marginally increases, the color of LE1 returns back to blue, reaching a value similar to that measured on +34 days. Over the remaining duration of the observations and as the LE brightness decreases in both the F438W and F547M, the color of LE1 slowly evolves back toward red. By +1991 days, the brightness and colors of LE1 are similar to those measured for LE3 and LE4, although LE2 appears marginally bluer.

3.3. Foreground Distance of the Scattering Dust Sheets

Following the single-scattering formalism (Couderc 1939; Patat 2005), the distance (z_{SM}) between a transient light source and a foreground LE-producing dust sheet can be inferred from the geometric relationship

$$z_{SM} = \frac{1}{2} \left(\frac{\rho_{ring}^2}{ct} - ct \right). \quad (1)$$

Here z_{SM} is the foreground distance to the scattering medium along the line of sight (LoS) in parsecs, c is the speed of light, t is the time since B -band maximum, and ρ_{ring} corresponds to the apparent ring radius in parsecs as projected on the sky and determined from the α values assuming the Cepheid distance to Cen A of 3.42 ± 0.18 (random) ± 0.25 (systematic) Mpc (Ferrarese et al. 2007). Measurements of ρ_{ring} and the inferred z_{SM} values for each LE component are plotted in Figure 4 and listed in Table A1. The z_{SM} values suggest the LEs are produced by dust sheets contained within a foreground volume extending between $z_{SM} \sim 60$ and 320 pc.

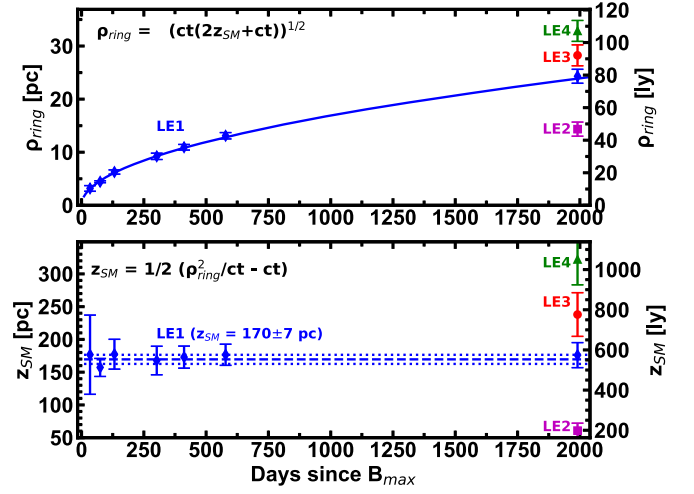


Figure 4. Top: values of ρ_{ring} for LE1–LE4. The blue line corresponds to the relation provided in the panel assuming for LE1 $z_{SM} = 170$ pc. Bottom: values of z_{SM} as inferred from Equation (1) for each LE component. The mean z_{SM} value and the associated uncertainty are indicated with dashed and dotted lines, respectively.

Sugerman (2003, their Equation (11)) provides a relation to estimate the thickness of a scattering dust sheet (Δz_{SM}) in terms of ρ , $\Delta\rho$, t , and an SN light-curve width parameter τ . Following Section A.5, we obtain for LE1 Δz estimates between 68–117 pc, while for LE2, LE3, and LE4 Δz values of 16 ± 5 pc, 32 ± 11 pc, and 38 ± 13 pc, respectively. These values, along with the compactness of the radial profiles of each LE, suggest they are formed by a single-scattering process that occurs in distinct dust sheets (Patat 2005; Yang et al. 2017).

4. Discussion

The color evolution of LE1 is perplexing though not unexpected given the totality of the dust lanes of Cen A as highlighted in Figure A3. We first turn to understand the color evolution in terms of the V -band effective optical depth (τ_{eff}^V) of the scattering dust sheets, while later consequences of dust reddening on the color evolution are considered. In doing so,

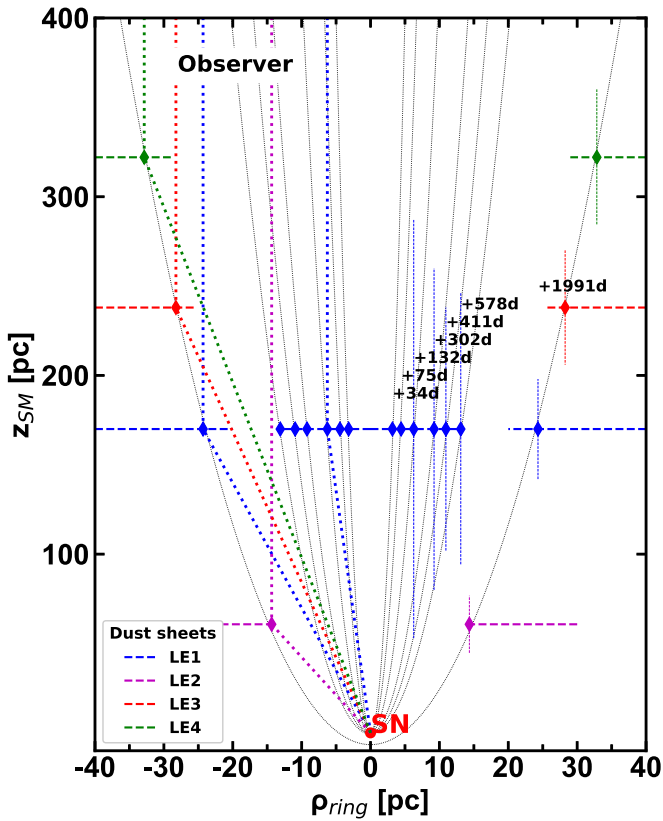


Figure 5. Schematic of multiple sheets of clumpy dust located along the LoS to Earth creating the various LE signatures of SN 2016adj. The parabolas indicate surface of equal light travel time to the observer. The horizontal dashed lines mark the z_{SM} inferred for the dust sheets producing the LEs, and the vertical dotted lines indicate their estimated widths (Δz_{SM}). Note that the sheets of dust do not necessarily extend symmetrically on both sides of the LoS.

relatively high τ_{eff}^V values are computed; however, after accounting for reddening, the values are consistent with the single scattering plus attenuation parameter space considered by Patat (2005).

Patat (2005, their Equation (21)) relates the observed LE color $(B - V)_{LE}$ to the intrinsic color $(B - V)_{SN_0, peak}$ of the SN at the peak following: $\tau_{eff}^V \approx 2.8[(B - V)_{LE} - (B - V)_{SN_0, peak}]$. Given the high and uncertain reddening parameters associated with SN 2016adj (M. D. Stritzinger et al. 2023, in preparation), we adopt $(B - V)_{SN_0} \approx 0.3 \pm 0.05$ mag (see Stritzinger et al. 2018, their Figure 5), which implies τ_{eff}^V values of 1.0 ± 1.0 to 2.8 ± 0.2 (see Table A1).

Returning to the apparent $(B - V)$ color evolution in Figure 3 of LE1 between epochs 1 and 2 and epochs 3 and 4, we find the abrupt changes in color are associated with changes in τ_{eff}^V . For example, LE1 abruptly evolves to the red as τ_{eff}^V increases from $\sim 1.0 \pm 1.0$ to 2.8 ± 0.2 . Similarly, the evolution of LE1 to the blue between epochs 2 and 4 occurs as τ_{eff}^V decreases from $\sim 2.8 \pm 0.2$ to 1.1 ± 0.2 . The color evolution to the blue could be due to changes of τ_{eff}^V and not due to geometrical effects coupled to the various wavelength dependencies. Such evolution is expected with steep density gradients and/or fluctuations in the dust distributed along the LoS, which leads to less self-absorption of blue photons and hence brighter/bluer LE emission (see Patat 2005).

The previous results assume that the apparent LE color is not affected by host-galaxy reddening. However, as indicated in

Figure A3, this is likely an incorrect assumption. In other words, the actual color of LE1 might be bluer and more similar to the segment located in the N direction than what is inferred from integrating the flux over the entire ring. The color from this segment is overplotted in the right-hand panel of Figure 3. Adopting these colors rather than those from the integrated flux of the ring, we infer an average τ_{eff}^V value of $\sim 0.6 \pm 0.4$. This is aligned with the range of values adopted by Patat (2005) in their single scattering plus attenuation model.

We now leverage the results gleaned from the analysis to construct the simple schematic of the 2D distribution of the dust sheets generating the LEs of SN 2016adj in Figure 5. The parabolas in the diagram correspond to the isodelay surfaces of the epochs of HST observations. The appearance of the LE components combined with our inferred z_{SM} values suggests that the dust within the scattering surfaces is distributed nonhomogeneously with significant “holes” within the sheets.

Within this scheme, LE1 is formed by a dense, clumpy layer of CSM located along the LoS extending over an area perpendicular to the isodelay surfaces of at least $\sim 28 \pm 10$ pc. LE3 and LE4 are formed by distinct dust sheets characterized by rather extensive holes relative to our LoS and first encountered by the scattering ellipsoid between +578 days and +1991 days. Turning to LE2, although this component exhibits the smallest z_{SM} value it does not appear until late times, which could also be due to a rather extensive hole within the sheet along the LoS.

5. Conclusion

We have presented a stunning set of HST images documenting the emergence and evolution of multiple LEs associated with SN 2016adj in Cen A, along with measurements of the brightness, color, and angular size on the sky of each LE component. Following the single-scattering formalism, a 2D schematic is constructed consisting of four discrete patchy dust sheets producing the echo components. Although beyond the scope of this Letter, one could apply a Heyney–Greenstein phase function analysis to construct an exquisite 3D mapping of the dust structures along the LoS and in doing so place constraints on the underlying dust properties (e.g., Yang et al. 2017). Finally, given the complex dust lane of Cen A, further HST images could not only document the evolution of the late LE components but also possibly reveal the emergence of additional LEs.

We are grateful to the reviewer for a thorough and timely review, which pointed out a handful of errors. This research is funded by grants from the Independent Research Fund Denmark (8021-00170B) and the Villum FONDEN (28021). M.F. is supported by a Royal Society—Science Foundation Ireland University Research Fellowship. L.G. acknowledges financial support from the MCIU AEI 10.13039/501100011033 PID2020-115253GA-I00 HOSTFLOWS project, the 2019 Ramón y Cajal program RYC2019-027683-I, the PIE project 20215AT016, and the program CEX2020-001058-M. Data presented in the paper were made with the NASA/ESA Hubble Space Telescope under program ID: 11360 (PI O’Connell), 14115 (PI Van Dyk), 14487 (PI Sugerman), 14700 (PI Sugerman), and 16179 (PI Filippenko). Images were retrieved from the archive at the Space Telescope Science Institute. STScI is operated by the Association of Universities for Research in Astronomy, Inc. under NASA contract NAS 5-26555. Support for S.S.L. via programs 14487 and 14700 was provided by NASA through a grant from the

Space Telescope Science Institute, which is operated by the Association of Universities for Research in Astronomy, Inc., under NASA contract NAS 5-03127.

Appendix Data Analysis Supporting Material

A.1. Recovering LE1 on +34 days

Figure A1 displays the +34 day F438W-band HST image of SN 2016adj prior to PSF subtraction (left panel) and after PSF subtraction (right panel). The PSF-subtracted image reveals LE1, which is the earliest detected LE documented in conjunction with an SN. Aperture photometry of the LE indicates a $\approx 12\%$ contribution to the total SN+ring flux in the F438W filter as measured from the unsubtracted image, while the LE recovered in the coeval F547M image contributes $\approx 2\%$.

A.2. Procedures to Measure the Angular Radius α

Measurements of α for each LE component were computed adopting the following procedure. First, the PSF of the SN was removed from the +34 day and +75 day images to minimize SN contamination, while this was not necessary in the later-epoch images. Next, two circles were drawn containing each LE on the host-subtracted images. Then, at each PA, the radius corresponding to the maximum intensity within the area delimited by the two circles encapsulating each LE component was determined and the median of these values serves as the best estimate of α . The associated uncertainty on α (and ρ_{ring}) corresponds to the median of the differences between the best radius fit and the maximum flux of the ring at each position angle. This error is propagated along with the error on the light-curve phase to estimate the uncertainties associated with estimates on z_{SM} .

A.3. On the Orientation of LE1's Dust Sheet

Following Tytenda (2004), a coincident position of the SN and the center of a LE ring suggests the dust slab producing the

ring emission is oriented perpendicular to our LoS. To verify whether or not the sheet of dust producing the LE ring associated with LE1 is indeed not inclined to our LoS, we performed the following. First, the brightest positions of LE1 in images obtained on +302 days and +412 days were fit with three different functions. This included a ring with the center fixed at the SN position, a ring with the center as a fit parameter, and an ellipse with the center as a free parameter. The functions produce good fits to the brightest regions of the LE with similar reduced chi-squared estimates. The best-fit ring and ellipse functions were both determined to have a center position coincident with that of the position of SN 2016adj to within 0.6 ± 0.1 and 0.6 ± 0.3 pixels, respectively. This exercise suggests that the sheet of dust-producing LE1 is oriented perpendicular to our LoS.

A.4. Surface Brightness of LE1

The top row of Figure A2 displays the LE flux versus PA of LE1 as measured from HST images obtained between +75 days to +1991 days, while the bottom row plots the corresponding F438W and F547M flux ratios. In cases when the diffraction spike from the bright star to the NW contaminated the LE emission, the aperture flux was extracted as a function of PA, and a correction was determined for the LE flux after removing the contamination by linear interpolation over the PA.

A.5. Estimating Δz

Following (Sugerman 2003, their Equation (11)), the thickness (Δz_{SM}) of a dust sheet producing an LE can be estimated in terms of ρ , $\Delta\rho$, t , and the light-curve width parameter τ . Estimates of $\Delta\rho$ were inferred from the FWHM measurements of the rings in the F438W-band images after integrating the ring flux at different radii over 360° . Depending on the epoch and on the LE, we obtained FWHM values between ~ 3 and 4 pixels. Assuming $\tau = 30$ days, Δz_{SM} values associated with the dust sheet producing LE1 from +132 days and +578 days range between

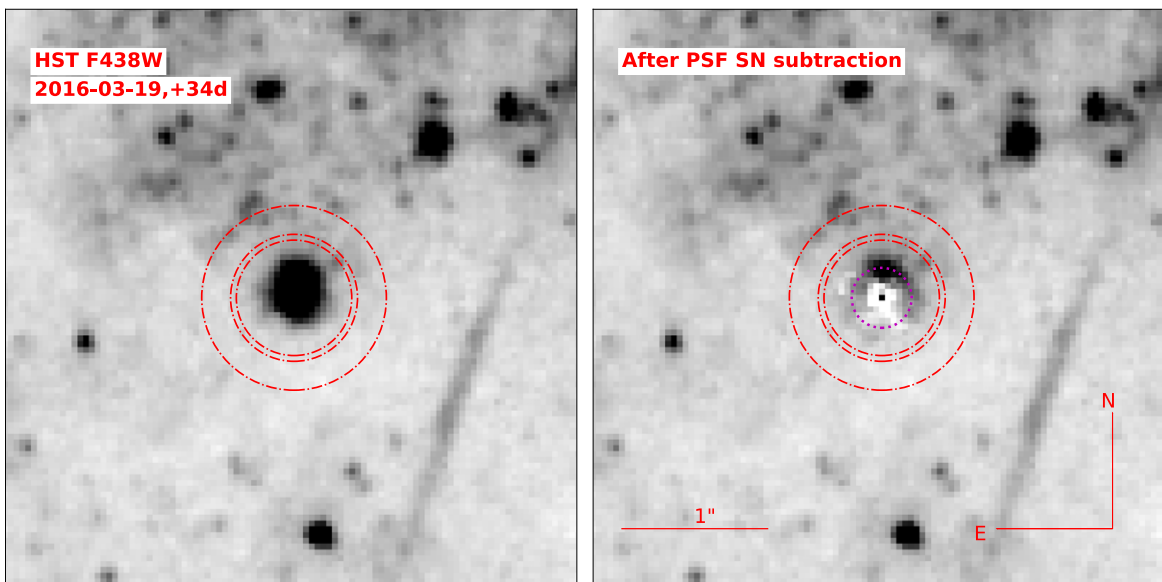


Figure A1. Left: HST F438W-band image of SN 2016adj obtained on +34 days. Right: residual image after subtraction of a PSF model constructed from two dozen stars. The emerging LE is indicated with a dotted magenta circle. Dashed-dotted red circles correspond to photometry and sky-background apertures. The scale and orientation of the images are reported in the right-hand panel.

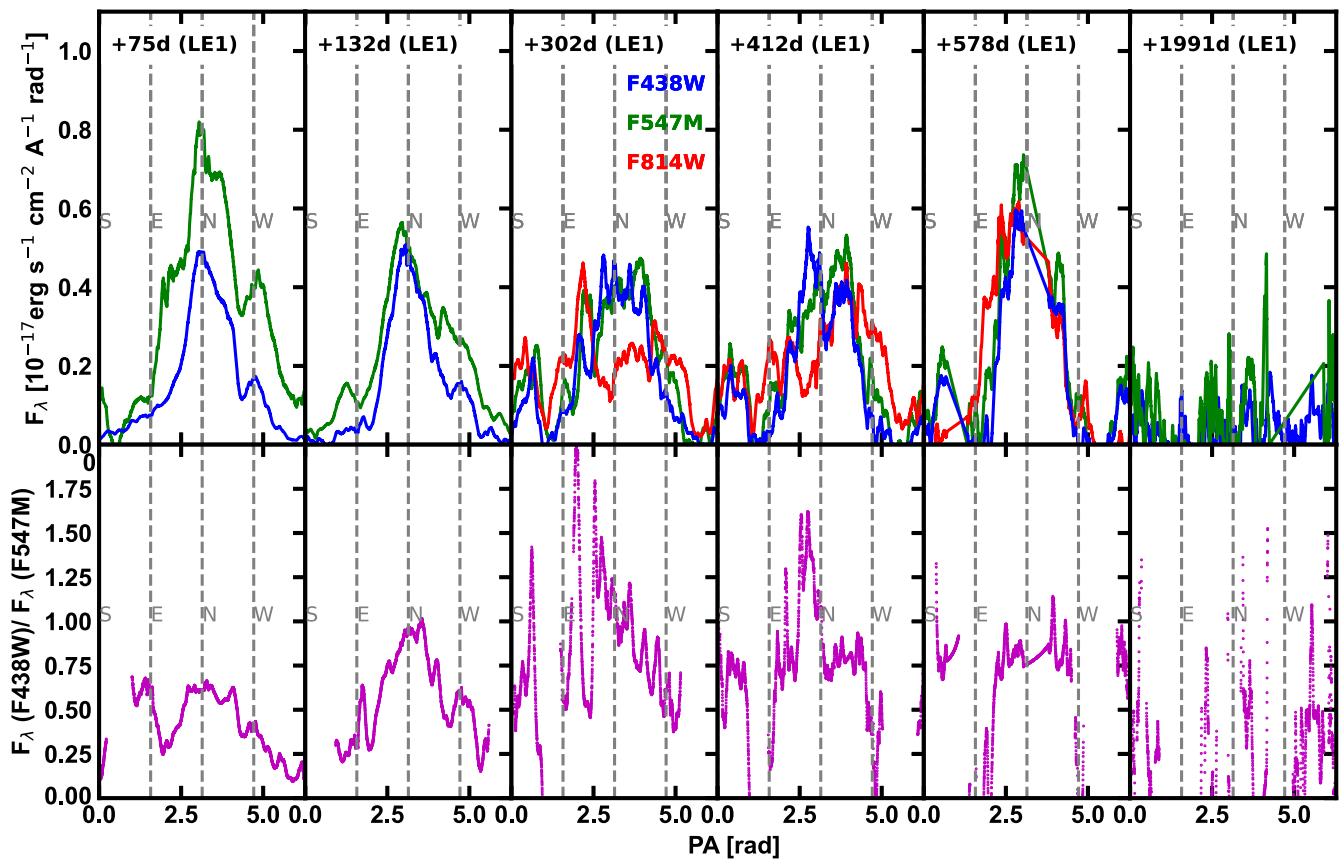


Figure A2. Top: fluxes of LE1 over six epochs plotted as a function of PA in two and/or three HST filters. Bottom: ratio of F438W- and F547M-band flux measurements as a function of PA.

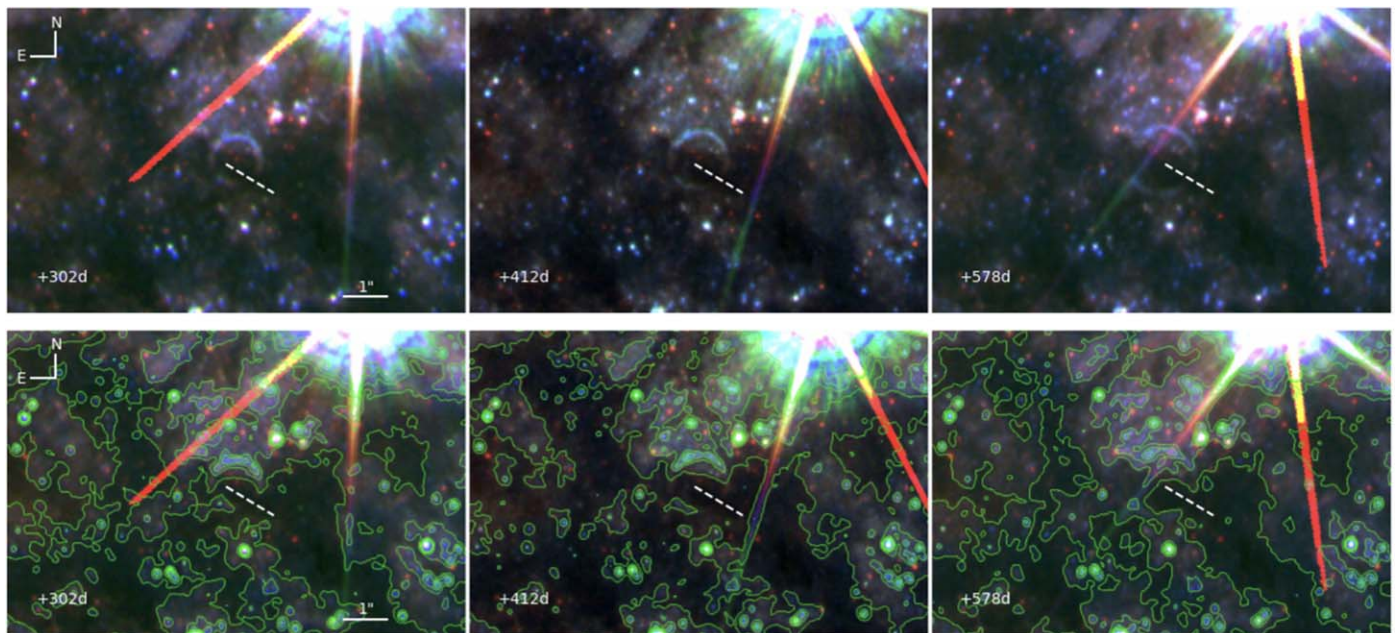


Figure A3. Top: composite RGB images centered on LE1 from epochs between +302 days and +578 days. A prominent dust lane indicated by a dashed white line and running E-NE to W-SW in the direction across the ring of LE1 clearly obscures both background stars and LE1 as it radially expands on the sky. The apparent color inferred from the total integrated flux is redder than the intrinsic color, which is more accurately traced by the segment of the ring extending from the N direction (see Figure A2). Bottom: the same images as in the top row but with contour lines superposed corresponding to different F438W-band flux levels. Regions of minimal contours trace the spectacular dust lanes covering the field of SN 2016aj.

Table A1
Light-echo Properties

Epoch	Phase ^a (days)	Angular Radius α ($''$)	ρ_{ring} (pc)	z_{SM} (pc)	Δz_{SM} (pc)	F_{F438W} ($^{\text{d}}$)	m_{F438W} (mag)	F_{F547M} ($^{\text{d}}$)	m_{F547M} (mag)	F_{F814W} ($^{\text{d}}$)	m_{F814W} (mag)	$\tau_{\text{eff}}^{\text{V}} \text{Ring}^{\text{b}}$	$\tau_{\text{eff}}^{\text{V}} \text{N}^{\text{c}}$
2 (LE1)	+34	0.19 ± 0.03	3.18 ± 0.53	176.68 ± 60.44	...	0.674 ± 0.135	22.34 ± 0.22	0.770 ± 0.154	21.70 ± 0.22	$1.0 \pm \mathbf{1.0}$...
3 (LE1)	+75	0.27 ± 0.01	4.44 ± 0.18	157.21 ± 13.74	...	0.993 ± 0.013	21.92 ± 0.01	2.069 ± 0.013	20.63 ± 0.01	$2.8 \pm \mathbf{0.2}$	2.0 ± 0.4
4 (LE1)	+132	0.38 ± 0.02	6.27 ± 0.40	177.41 ± 22.79	117 ± 2	0.884 ± 0.013	22.05 ± 0.02	1.377 ± 0.013	21.07 ± 0.01	$1.9 \pm \mathbf{0.2}$	0.6 ± 0.3
5 (LE1)	+302	0.56 ± 0.04	9.22 ± 0.60	167.80 ± 21.79	90 ± 2	1.062 ± 0.021	21.85 ± 0.02	1.253 ± 0.019	21.17 ± 0.02	1.20 ± 0.02	20.38 ± 0.02	$1.1 \pm \mathbf{0.2}$	0.1 ± 0.2
6 (LE1)	+412	0.66 ± 0.03	10.94 ± 0.53	172.97 ± 16.84	68 ± 2	1.019 ± 0.021	21.89 ± 0.02	1.252 ± 0.025	21.18 ± 0.02	1.30 ± 0.03	20.29 ± 0.02	$1.2 \pm \mathbf{0.2}$	0.3 ± 0.2
7 (LE1)	+578	0.79 ± 0.04	13.10 ± 0.60	176.56 ± 16.14	76 ± 2	1.117 ± 0.027	21.79 ± 0.03	1.453 ± 0.054	21.01 ± 0.04	1.29 ± 0.14	20.31 ± 0.11	$1.3 \pm \mathbf{0.3}$	1.4 ± 0.4
8 (LE1)	+1991 ^e	1.47 ± 0.08	24.31 ± 1.31	175.98 ± 19.12	28 ± 10	0.221 ± 0.051	23.55 ± 0.25	0.411 ± 0.027	22.39 ± 0.07	$2.4 \pm \mathbf{0.9}$...
8 (LE2)	+1991 ^e	0.87 ± 0.08	14.35 ± 1.33	60.76 ± 11.40	16 ± 5	0.289 ± 0.041	23.26 ± 0.16	0.371 ± 0.049	22.50 ± 0.14	1.3 ± 0.7	...
8 (LE3)	+1991 ^e	1.70 ± 0.12	28.25 ± 1.97	237.98 ± 33.32	32 ± 11	0.242 ± 0.059	23.45 ± 0.27	0.421 ± 0.032	22.36 ± 0.08	$2.2 \pm \mathbf{0.9}$...
8 (LE4)	+1991 ^e	1.98 ± 0.12	32.85 ± 1.97	322.06 ± 38.75	38 ± 13	0.188 ± 0.068	23.72 ± 0.41	0.301 ± 0.037	22.72 ± 0.13	$2.0 \pm \mathbf{1.4}$...

Notes. The uncertainties in the flux measurements of the first two epochs include a conservative 20% uncertainty given the contaminating residuals created by our PSF SN subtraction. The F438W, F547M, and F814W filters are similar to ground-based *BVi* filters. The magnitudes are reported in the AB system.

^a Days past the epoch of the *B*-band maximum.

^b Values computed adopting colors computed from the full LE ring. The quoted uncertainties account for the 0.05 mag error in the adopted intrinsic SN peak color, and the observational errors of the apparent color of the ring.

^c Values computed adopting colors computed from the northern bright segment of LE1.

^d $10^{-17} \text{ erg s}^{-1} \text{ cm}^{-2} \text{ \AA}^{-1}$.

^e For the last epoch measurements are reported for LE1, LE2, LE3, and LE4. At this epoch, the filter F547M is actually F555W.

$\Delta z_{SM} = 68 \pm 2$ pc $\Delta z_{SM} = 117 \pm 2$ pc. Here the associated errors account for the uncertainty in the measured FWHM values of each ring. The LEs observed at the last epoch show the FWHM of the rings between 2 and 4 pixels, corresponding to values of $\Delta z_{SM} = 16 \pm 5$ pc for LE2, $z_{SM} = 32 \pm 11$ pc for LE3, and $z_{SM} = 38 \pm 13$ pc for LE4. All z_{SM} and Δz_{SM} estimates are provided in Table A1.

A.6. RGB Image of LE1 of SN 2016adj

Composite RGB (red, green, blue) images constructed by aligning and stacking HST images obtained on +302 days, +412 days, and +578 days are shown in the top row of Figure A3. The bottom row displays the same images with the superposed intensity of contours corresponding to the F438W-band flux, with regions lacking contours tracing the complex dust lanes extending across the field.

A prevalent dust lane running in the E–NE to W–SW direction and across LE1, reveals significant attenuation of both background stars and the LE1 as it radially expands on the sky. Clearly, there is a significant amount of dust at a very large distance (>1000 pc) in front of the position of SN 2016adj and has a large thickness along the z -axis. This host dust could be a single structure or multiple layers and surely contributes to the large host visual extinction inferred from the analysis of the SN colors (M. D. Stritzinger et al. 2023, in preparation). This extended dust structure could still allow for a relatively low density of dust in the close-in sheet producing LE1, allowing that dust to remain in the single-scattering regime. The photons we are seeing as LE1 all traveled in a straight line from the SN to the dust sheet producing LE1 and only suffered one scattering there to be directed into our LoS to Earth. The distant foreground dust is dimming these LE photons, but if it is far enough in the foreground and extended over a long depth along the LoS, the LE it would produce from photons that traveled directly from the SN would be faint, at large radii, and diffusely smeared out and possibly too faint to be detected.

ORCID iDs

Maximilian D. Stritzinger  <https://orcid.org/0000-0002-5571-1833>

Francesco Taddia  <https://orcid.org/0000-0002-2387-6801>

Stephen S. Lawrence  <https://orcid.org/0000-0002-7491-7052>

F. Patat  <https://orcid.org/0000-0002-0537-3573>

Morgan Fraser  <https://orcid.org/0000-0003-2191-1674>

Lluís Galbany  <https://orcid.org/0000-0002-1296-6887>

Simon Holmbo  <https://orcid.org/0000-0002-3415-322X>

Ali Hyder  <https://orcid.org/0000-0002-3350-4243>

Emir Karamehmetoglu  <https://orcid.org/0000-0001-6209-838X>

References

- Banerjee, D. P. K., Joshi, V., Evans, A., et al. 2018, *MNRAS*, **481**, 806
- Bond, H. E., Henden, A., Levay, Z. G., et al. 2003, *Natur*, **422**, 405
- Bradley, L., Sipőcz, B., Robitaille, T., et al. 2020, *astropy/photutils*: 1.0.0, 1.0.0, Zenodo, doi:[10.5281/zenodo.4044744](https://doi.org/10.5281/zenodo.4044744)
- Chevalier, R. A. 1986, *ApJ*, **308**, 225
- Couderc, P. 1939, *AnAp*, **2**, 271
- Crotts, A. P. S. 1988, *ApJL*, **333**, L51
- Ferrarese, L., Mould, J. R., Stetson, P. B., et al. 2007, *ApJ*, **654**, 186
- Havlen, R. J. 1972, *A&A*, **16**, 252
- Hounsell, R. A., Miller, J. A., Pan, Y. C., et al. 2016, *ATel*, **8663**, 1
- Hyder, A., Lawrence, S., & Sugerman, B. 2018, *AAS Meeting*, **231**, 257.04
- Kapteyn, J. C. 1901, *AN*, **157**, 201
- Kiyota, S., Shappee, B. J., Stanek, K. Z., & Dong, S. 2016, *ATel*, **8654**, 1
- Marples, P., Bock, G., & Parker, S. 2016, *ATel*, **8651**, 1
- Patat, F. 2005, *MNRAS*, **357**, 1161
- Rest, A., Foley, R. J., Sinnott, B., et al. 2011, *ApJ*, **732**, 3
- Rest, A., Matheson, T., Blondin, S., et al. 2008, *ApJ*, **680**, 1137
- Rest, A., Prieto, J. L., Walborn, N. R., et al. 2012, *Natur*, **482**, 375
- Ritchey, G. W. 1901, *ApJ*, **14**, 293
- Shahbandeh, M., Hsiao, E. Y., Ashall, C., et al. 2022, *ApJ*, **925**, 175
- Stritzinger, M., Hsiao, E. Y., Morrell, N., et al. 2016, *ATel*, **8657**, 1
- Stritzinger, M. D., Taddia, F., Burns, C. R., et al. 2018, *A&A*, **609**, A135
- Sugerman, B., & Lawrence, S. 2016, *ATel*, **8890**, 1
- Sugerman, B. E. K. 2003, *AJ*, **126**, 1939
- Suntzeff, N. B., Heathcote, S., Weller, W. G., Caldwell, N., & Huchra, J. P. 1988, *Natur*, **334**, 135
- Swope, H. H. 1940, *BHarO*, **913**, 11
- Thomas, A., Tucker, B. E., Childress, M., et al. 2016, *ATel*, **8664**, 1
- Tylenda, R. 2004, *A&A*, **414**, 223
- Valenti, S., Elias-Rosa, N., Taubenberger, S., et al. 2008, *ApJL*, **673**, L155
- Vogt, F. P. A., Besel, M.-A., Krause, O., & Dullemond, C. P. 2012, *ApJ*, **750**, 155
- Xu, J., Crotts, A. P. S., & Kunkel, W. E. 1995, *ApJ*, **451**, 806
- Yang, Y., Wang, L., Baade, D., et al. 2017, *ApJ*, **834**, 60
- Yi, W., Zhang, J.-J., Wu, X.-B., et al. 2016, *ATel*, **8655**, 1